Identification of Key Interactions in the Initial Self-Assembly of Amylin in a Membrane Environment

Journal:	*Biochemistry*
Manuscript ID	bi-2017-00344a.R2
Manuscript Type:	Article
Date Submitted by the Author:	n/a
Complete List of Authors:	Christensen, Mikkel; Aarhus University, Department of Chemistry Skeby, Katrine; Aarhus University, Department of Chemistry Schiøtt, Birgit; Aarhus University, Department of Chemistry

Identification of Key Interactions in the Initial Self-Assembly of Amylin in a Membrane Environment

Mikkel Christensen[1,2], *Katrine K. Skeby*[1], *Birgit Schiøtt*[1]*

[1]Interdisciplinary Nanoscience Center (iNANO), and Department of Chemistry, Aarhus University

[2]Sino-Danish Center for Education and Research

To whom correspondence should be addressed. Tel. 87155975. E-mail: Birgit@chem.au.dk.

Birgit Schiøtt ORCID: 0000-0001-9937-1562

ABBREVIATIONS:

IAPP, Islet Amyloid Polypeptide; T2DM, Type II Diabetes Mellitus; HMMM, Highly Mobile Membrane Mimetic; NMR, Nuclear Magnetic Resonance; CD, Circular Dichroism; ThT, Thioflavin T; EM, Electron Microscopy; MD, Molecular Dynamics; AFM, Atomic Force Microscopy; PS, phosphatidylserine; PG, phosphatidylglycerol; PC, phosphatidylcholine; SDS, Sodium Dodecyl Sulfate; DVPC, divalerylphosphatidylcholine; DVPS, divalerylphosphatidylserine; DCLE, 1,1-Dicloroethane.

ABSTRACT

Islet Amyloid Polypeptide (IAPP), also known as amylin, forms aggregates that reduce the amount of insulin-producing cells in patients with type II diabetes mellitus (T2DM). Much remains unknown about the process of aggregation and cytotoxicity, but it is known that certain cell-membrane components can alter the rate of aggregation. Using atomistic molecular dynamics simulations combined with the Highly Mobile Membrane Mimetic (HMMM) model incorporating enhanced sampling of lipid diffusion, we investigate amylins interaction with the membrane components as well as the self-assembly of amylin. Consistent with experimental evidence we find that an initial membrane bound α-helical state folds into stable β-sheet structures upon self-assembly. Our results suggest the following mechanism for the initial phase of amylin self-assembly: The peptides move around on the membrane with the positively charged N-terminal interacting with the negatively charged lipid head-groups. When the peptides start to interact, they partly unfold and break some of the contacts with the membrane. The initial interactions between the peptides are dominated by aromatic and hydrophobic interactions. Oligomers are formed showing both intra- and inter-peptide β-sheets, initially with interactions mainly in the C-terminal domain of the peptides. Lowering the pH to 5.5 is known to inhibit amyloid formation. At low pH, His18 is protonated adding a fourth positive charge at the peptide. With His18 protonated no oligomerization is observed in the simulations. The additional charge gives a strong mid-point anchoring of the peptides to negatively charged membrane components and the peptides experience additional inter-peptide repulsion, hereby preventing interactions.

INTRODUCTION

Human Islet Amyloid Polypeptide (hIAPP), also known as amylin, is a small hormone peptide. The peptide forms amyloid aggregates in patients with type II diabetes Mellitus (T2DM) and deteriorates the disease. T2DM is a multifactorial disease, generally characterized by a decrease in insulin response and decreased secretion of insulin caused by loss of β-cells. Amylin is stored along with insulin in the secretory granules of the β-cells in the pancreatic islets and released together with insulin as response to elevated levels of blood-glucose.[1] The physiological role of amylin is unclear; however it is thought to have multiple regulatory roles, including inhibition of gastric emptying, food intake and glucagon secretion.[2] Presence of amyloid fibrils have been identified on the islet cells of the pancreas in patients with T2DM[3] which has been correlated with a loss of the insulin producing β-cells.[4] It is therefore a widely accepted theory that the aggregation of amylin has a causal relationship to the loss of β-cells.[5,6] The fibrillation of amylin is not the primary cause of T2DM, however it is found to be a contributing factor and responsible for the decreased overall insulin production from the β-cells.[7,8] While the correlation between the formation of amyloid fibrils and loss of β-cells is well established, the molecular mechanism of the cytotoxic effect of the aggregates remains unclear. Some research indicates that it is the mature fibrils that destroy the cell membrane,[9,10] while other studies indicate that the cell disruption is caused by the formation of toxic oligomers.[11] The oligomer hypothesis is supported by the finding of non-selective ion-channels of amylin oligomers, which has been characterized by AFM,[12] electrochemical measurements,[13] as well as leakage of content from lipid vesicle.[10,14-16]

Amylin is a 37-residue polypeptide; in the physiological form it has a disulfide bridge between residues Cys2 and Cys7 and an amidated C-terminus. At physiological pH it carries a +3 charge, from the N-terminus, Lys1, and Arg11. The sequence is shown in **Figure 1**.

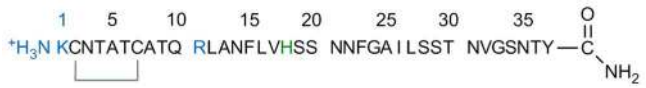

Figure 1: Sequence of amylin. The disulfide-bridge between Cys2 and Cys7 is indicated with a line. The three positive charges present at physiological pH are indicated with a blue color of residue letters. His18 is shown in green. The N- and C-termini including capping are shown at the ends.

His18 is expected to be neutral at physiological pH, and protonated hence carrying a positive charge at lower pH values.[17] The amylin peptide is intrinsically disordered, meaning that it does not have a well-defined structure in solution as a monomer, however mostly it alternates between random coil and α-helix, as revealed by nuclear magnetic resonance (NMR) and circular dichroism (CD) spectroscopy.[18,19] When bound to a membrane or in membrane mimicking environments (such as bound to micelles or dissolved in hexaflouroisopropanol) the secondary structure of the peptide becomes primarily α-helical.[20-22] Furthermore, different experimental methods yielding atomic details have been applied to obtain structural information about the peptide: The α-helical structures of amylin bound to sodium dodecyl sulfate (SDS) micelles have been determined in atomic detail using constraints from NMR spectroscopy. One structure has been determined at pH 4.6 and without the C-terminal amidation[23] another at physiological pH 7.4 and including the amidated C-terminus.[24] Both NMR-ensembles reveal α-helical conformations and the major structural difference is that the former is extended, while the latter

has a kink around residue Ser20. Under certain conditions the peptides aggregate into β-sheet fibrils after a lag-phase: The fibril formation has been characterized using CD spectroscopy, Thioflavin-T (ThT) binding assays, and electron microscopy (EM).[25,26] Detailed information about the structure of fibrils formed in solution has been obtained with solid-state NMR suggesting in-register, parallel β-sheets between the peptides in the fibril with a turn between His18 and Phe23.[27] A β-hairpin intermediate has been proposed to mediate the transition to β-sheet fibrils, the proposed β-hairpin (**Figure 2a)** has a turn at the same place as the proposed fibril structure (**Figure 2b)**.[28,29]

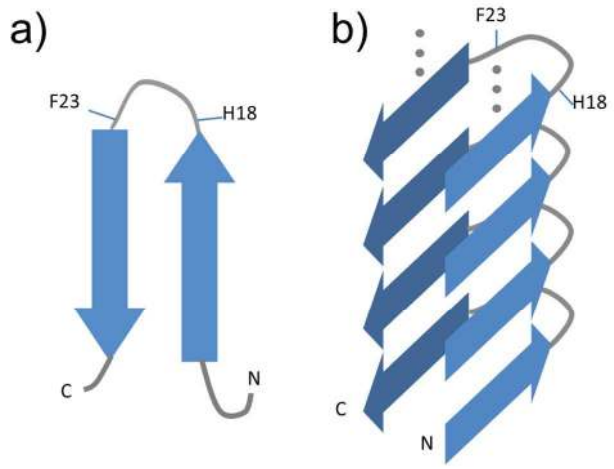

Figure 2: a) Proposed β-hairpin structure of amylin. The hairpin contains the same β-strand regions as the fibril as well as the same turn; however the β-sheet is formed by two-parts of the same peptide. b) Schematic representation of the amylin fibril structure as proposed from solid-state NMR spectroscopy. Each peptide is illustrated as two β-strands connected by a turn at residues H18 to F23. The segments of the β-strands are interacting with the same segments on the adjacent peptides. The dots indicate the directions of fibril extension.

Experimental evidence suggests that membrane composition influences the rate of amyloid formation and membrane disruption. Negatively charged lipids, such as phosphatidylserine (PS) and phosphatidylglycerol (PG) lipids, have been shown to increase the rate of aggregation *in vitro* by CD spectroscopy, Thioflavin-T (ThT) binding assays[30] and x-ray diffration.[31] The studies indicate that the membrane induces conformational changes in the peptides and catalyzes the amyloid fibril formation. The highest increase in aggregation rate has been observed using a 25-30mol% of anionic lipids in the membrane.[31,32] Gangliosides have similarly been shown to increase the aggregation rate. Ganglioside lipids are glycolipids carrying a net negative charge. It is seen by cell staining experiments that amylin interacts with domains enriched in gangliosides, thus giving a high local concentration of amylin leading to increased aggregation.[33] However, recent studies with amyloid-β have indicated that depending on the ganglioside concentration the rate of oligomerization either increase or decrease, this could potentially be the case for amylin as well.[34] Studies have shown that the cholesterol content of the membrane similarly can affect the aggregation rate. Depending on the conditions and concentration it can either increase or decrease the aggregation rate.[35-37] Infrared reflection absorption spectroscopy experiments indicates that the N-terminal part of the peptide interacts with the negatively charged lipids.[38] In the secretory granules of the pancreatic β-cells, the pH is approximately 5.5.[39] At such acidic conditions the fibril formation and membrane damage is inhibited in vesicles containing 30% anionic PS lipids and 70% zwitterionic phophatidylcholine (PC) lipids as revealed by dye-leakage experiments, CD spectroscopy, and ThT fluorescence.[17] Residue His18 is expected to become positively charged at low pH, and this was hypothesized by the authors to be the cause of the observed lower aggregation rate, possibly due to the increased repulsion between the charged peptides.[17,40]

The biophysical methods for studying the rate of protein aggregation and fibril morphology include ThT-fluorescence, CD spectroscopy, AFM, and EM.[41] However, unlike molecular dynamics (MD) simulations, these methods are not capable of investigating the detailed structural changes that occur in the initial transition from monomeric peptides to oligomer aggregates, due to the rapid aggregation of amylin. The self-assembly of amylin in solution has previously been investigated using replica exchange MD[42] and similarly for amyloid-β peptides.[43] Both studies revealed a transition from α-helical monomers to β-sheet containing oligomers. Monomeric ensembles of the amylin$_{1\text{-}19}$ fragment[40] and full length amylin[44] bound to lipid bilayers have been investigated using MD simulations, and the studies found that this environment stabilized the N-terminal α-helix. Oligomer species based on the proposed fibril structures in a membrane environment have been simulated in a suggested membrane penetration setup, showing that this structure is stable in a membrane environment and form a water channel across the bilayer.[44] To study fibril growth the assembly of protofibrillar fragments of amylin has been investigated with coarse-grained MD simulations.[45]

Herein, we apply MD simulations to characterize the self-assembly of amylin peptides bound to lipid membranes in atomistic details. Capturing large conformational changes of proteins and peptides such as unfolding and assembly of peptides at the timescales of MD simulations poses a sampling problem.[46] Interactions with lipid membranes usually slow down the peptide dynamics, and hence conformational sampling of peptides is limited due to the slow diffusion of the lipids and the high number of interactions between the lipid head groups and the peptides. To partly overcome this issue, the HMMM model has been developed by Tajkhorshid and co-workers.[47] This model substitutes the hydrophobic interior of the membrane with an organic solvent 1,1-dichloroethane (DCLE) that mimics the hydrophobic properties of the lipid tails in membrane

core. The membrane-water interface is represented with short-tailed lipids. While this drastically increases the lipid diffusion and hence provides better sampling, it retains atomistic detail at the membrane surface. The HMMM model is able to reproduce the energetics of protein insertion into full-length lipid membranes[48] and it has been successfully applied in capturing the binding and insertion of a series of proteins, e.g. α-synuclein,[49] influenza virus hemagglutinin fusion peptide,[50] cytochrome P450,[51] and amylin.[52]

COMPUTATIONAL METHODS

The starting coordinates for the MD simulations were extracted from representative membrane bound structures of an amylin monomer from a previous study of each tautomer and protonation state of His18 (**Figure 3a**).[52] Amylin is modelled in its physiological form with amidated C-terminus and the disulfide-bridge between Cys2 and Cys7 present. The systems were replicated in both bilayer dimensions resulting in four identical copies of the original conformation (**Figure 3b**). The membrane bound structures are judged to have adapted to the condition of being bound to phospholipid bilayers, and are therefore the best available starting point for the simulations. The membrane bound peptides show similar conformations to the NMR structure of SDS bound amylin[24], although the C-terminal half of the peptide is less structured after bilayer exposure.

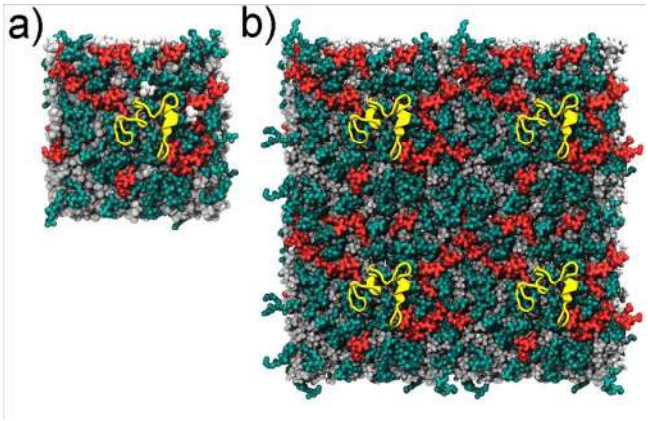

Figure 3: a) End structure of amylin bound to membrane from previous study[52] and b) starting setup for molecular dynamics simulations with 4 peptides on a membrane. The PC lipids are shown in green, the PS lipids are shown red, DCLE in gray, and the peptides are shown in yellow.

A 7:3 ratio of dioleoylphosphatidylserine (DOPS) and dioleoylphosphatidylcholine (DOPC) lipids was chosen for the membrane, since this content of anionic lipids is known to accelerate the amyloid formation of amylin *in-vitro,*[32,53] hence providing directly comparable computational and experimental data. To enhance diffusion the membrane was modelled with the HMMM model containing 30% anionic divalerylphosphatidylserine (DVPS) and 70% zwitterionic divalerylphosphatidylcholine (DVPC) and a membrane core of 1,1-dicloroethane (DCLE), this setup captures the essential properties of a membrane composed of DOPC and DOPS.[47] The system was solvated in CHARMM modified TIP3P water[54-56] and ions are present to neutralize the system. Because the lipids are soluble in water due to their relatively short tails, they were constrained in the direction perpendicular to the membrane with a weak harmonic force constant of $0.05\frac{kcal}{mol\ Å^2}$ acting on the carbonyl carbons of the lipid tails in the simulations, similar to the advice given in the original HMMM paper.[47] A system was built from membrane bound structures of amylin using for each of the two neutral tautomers of His18, with the hydrogen

placed at Nδ and Nε, respectively, and for the positively charged His18. The simulations were performed for 400 ns each in three repeats, yielding a total of 3.6 μs of atomistic simulation. The setups are summaries in **Table 1**.

Table 1: Overview of MD simulation setup

His 18 Tautomer	His 18 Protonation state	No. of simulations	Time pr. simulation (ns)
Nδ	Neutral	3	400
Nε		3	400
-	Charged	3	400

SIMULATION CONDITIONS

All simulations were performed using the GROMACS 5.0.2 MD engine[57] and the CHARMM36 force field[58] for the lipids and the CHARMM22* force field[59] for the peptides. The latter force field has proven optimal for reproducing a balance between secondary structure elements of amylin consistent with experimental data,[60] recently this was also shown for the similar amyloidogenic peptide amyloid-β, [61] and furthermore it generally performs well for intrinsically disordered peptides. [59] The bond lengths related to hydrogens were constrained with the LINCS algorithm[62] and the simulations were performed with a 2 fs time step. The temperature was held at 310 K with the velocity rescaling algorithm[63] and a pressure of 1 atm was achieved with the Parinello-Rahman[64] pressure coupling barostat with a coupling constant of 1 ps. The pressure coupling was applied semi-isotropically with the x-y dimensions fixed and volume regulation in the z-direction. The x-y area was set to maintain an area per lipid around 8% higher than equilibrium for full length DOPC and DOPS lipids, such as recommended for the HMMM

model, to facilitate potential peptide insertion without increasing the surface tension. The electrostatic interactions were calculated using the Particle Mesh Ewald algorithm[65] with a grid spacing of 0.1 nm and a short-range cutoff of 1.2 nm. The van der Waals interactions were modified with a force-switch cutoff[66] from 1.0 to 1.2 nm.

RESULTS AND DISCUSSION

This study investigates the self-assembly of monomeric amylin peptides into oligomers to mimic the initial phases of amyloid fibril formation. Simulations have been performed in atomistic details using 4 monomers of amylin on a membrane consisting of 70% PC and 30% PS lipids modelled with the HMMM model.[47] Three simulations for each of the two neutral tautomers of His18 were run for 400 ns each and with 4 peptides in each system, which amounts to 24 single peptide trajectories in total. In addition 3 simulations of 400 ns were performed with a cationic histidinium at His18 entailing 12 peptide trajectories. From an overall visual analysis of the simulations it was observed that many of the peptides with the neutral His18 interacted persistently with other peptides during the simulations, while peptides with cationic His18 did not make inter-peptide contacts, or only briefly made contact to other peptides, and therefore mostly sampled monomeric membrane-bound conformations. In some of the His-neutral simulations all the peptides where included in self-assembly (Movie S1) and in other simulations 2 or 3 of the peptides assembled (Movie S2). In the simulations with cationic His18, none of the peptides make lasting contact with other peptides (Movie S3). The oligomers formed in the self-assembly simulations were rather heterogeneous overall, but they do allow for an investigation of trends regarding the structure and the type of interactions formed between the peptides.

The primary focus of this study is on the process of self-assembly of amylin, thus the analysis will only include data from the peptides that show durable interaction with other peptides. The

distribution of the number of residues of the peptides in contact with other peptides is shown in **Figure 4**, with contact defined as two heavy atoms of the respective residues being within 5 Å. The distribution for all the peptides in all simulations peaks around 16 residues (black in **Figure 4)** in contact with other peptides, which indicates that the individual peptides have a tendency to have 16 residues interacting with other peptides. From the peak the distribution decrease smoothly to a higher number of contacts, but it is increased and noisy moving to lower values. The low contact numbers include transient contacts that do not represent aggregated structures. To focus the analysis on the aggregated peptides the peak is fitted to a normal distribution (fitted to a Gaussian function with parameters for the mean, μ=15.7, and standard deviation, σ=5.5; green in **Figure 4**) and all peptides that are not above the first lower standard deviation (rounded down to 10) in more than half the simulation time are not included in the analysis. 17 peptides had more than 10 residues in contact with other peptides in more than half the simulations time, these were chosen for analysis. The contact distribution for the 17 peptides chosen for analysis is in good agreement with the fitted Gaussian (orange in **Figure 4)**. The excluded peptides peak at around 3 residues in contact with other peptides (yellow in **Figure 4)**. A similar distribution is observed for the peptides with cationic His18 (blue in **Figure 4)**. None of the peptides with cationic His18 are included in the analysis, as only one pair of peptides had a high number of residues in contact, but with duration less than half the simulation time. The time-evolution of the number of residues in contact with other peptides for the individual peptides is shown in **Figure S1**.

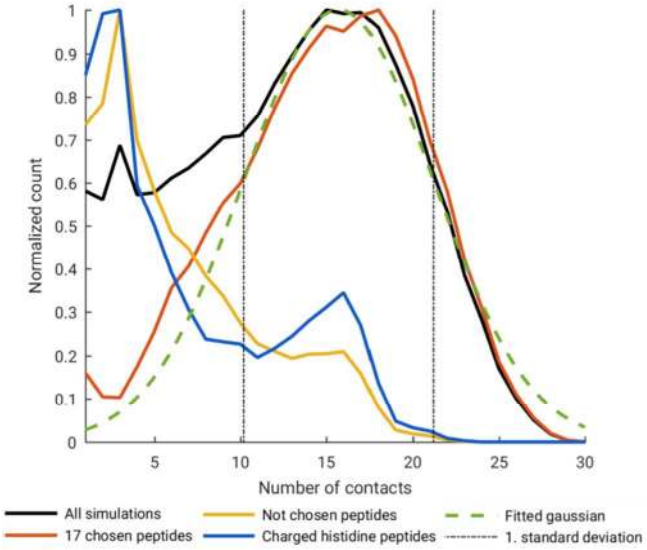

Figure 4: Distributions of the number of residues in contact with other peptides for all simulations (black), 17 chosen peptides (red), not chosen peptides (yellow), and peptides with cationic His18 (blue). The peak of the distribution with all peptides is fitted to a Gaussian function (green) and the first standard deviation (upper and lower, dashed lines) of this function is indicated.

The following quantitative analysis will include a discussion of the interactions between the peptides, the conformational changes related to the self-assembly and the peptide-lipid interactions. The peptides with cationic His18 will be treated separately in the analysis. The simulations with the neutral tautomers of His18 will be analyzed together, as no particular differences were observed between the tendency of the peptides to self-assembly from the visual analysis or from the contact analysis in **Figure S1**.

Interactions between the neutral peptides during self-assembly

During the simulations many of the peptides acquired notable contacts with other peptides. The time-evolution of the fraction of each residue in contact with other peptides is shown in **Figure 5a** with contact defined as any heavy atom of the two residues being within 5 Å. Within the first 50 ns of the simulations, less than 10% of any residue in the 17 peptides was in contact with other peptides in the simulations. The first distinctive residues to show contacts were Phe15 and Phe23, which after 50 ns had contact to other peptides in more than 50% of the 17 peptides. After 100 ns many of the residues from 10 to 37 were in contact with other peptides in a high fraction of the peptides. Still residues Phe15 and Phe23 had the most dominating contacts to other peptides. After 200 ns, contacts with the aromatic residues Phe15, His18, and Tyr37 are still prominent, and interactions with residues 22-NFGAIL-27 are dominating the interactions with more than 80% of the residues in contacts with other peptides.

The residue-residue contact map in **Figure 5b** shows which residues are in contact with which residues in other peptides averaged over all the contacts observed during the simulations for the 17 aggregating peptides. Starting at residue Ser20 a diagonal is observed, showing parallel interaction ending around residue Thr30, this shows that these residues have in-register contacts, meaning that these residues have a tendency to interact with the same residue index of the other peptides. The interactions of residue Phe15 are indicated on the contact map in **Figure 5b**. Phe15 has sustained interactions with Phe15 on other peptides and also with the hydrophobic residues in other parts of the sequence, predominantly with Ala25 and Ile26, but also the C-terminal residues Asn35, Thr36, and Tyr37. Residue Phe23 is found to have stable interactions with Phe23 on other strands and with His18, as encircled in **Figure 5b**. Generally the inter-peptide contacts are between the residues in the C-terminal part. The N-terminal residues 1-10 had

almost no interactions with other peptides; this is primarily due to interactions with the membrane, which will be analysed in greater detail later.

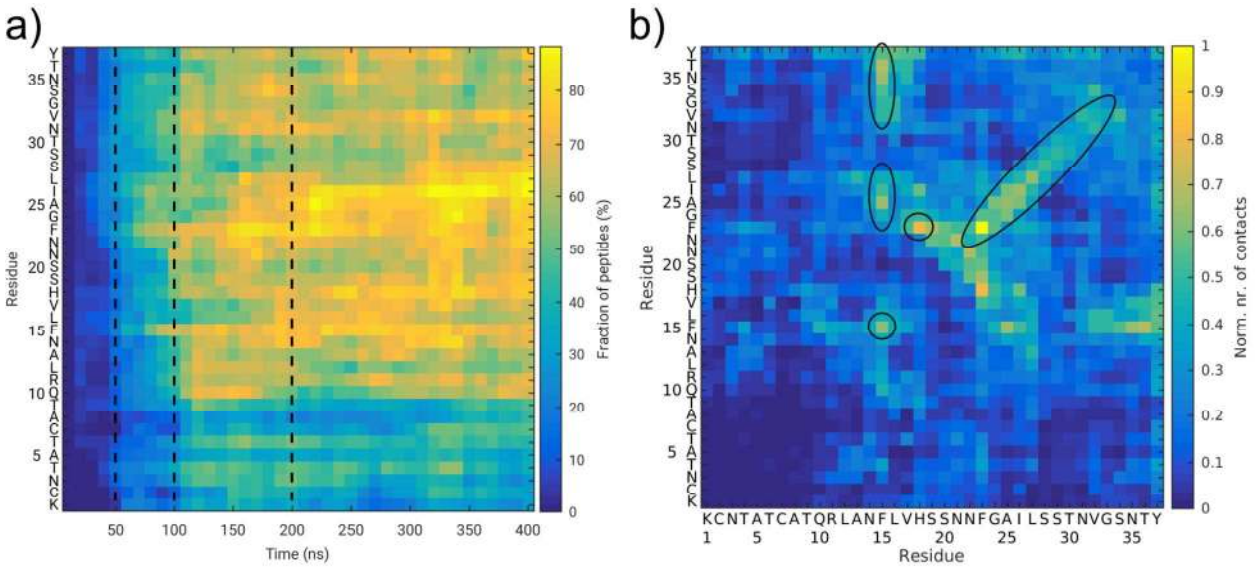

Figure 5: a) Fraction of residues of the 17 peptides that are in contact with other peptides as a function of simulation time. The data is plotted in averaged windows of 10 ns. The first dashed line indicates 50 ns, the second indicates 100 ns, and the third indicates 200 ns. A contact is defined between residues for which any pair of atoms from the two residues in question is within 5 Å. b) Number of contacts between a residue in one strand and residues in any of the remaining peptides summed over all 17 peptides. The number is normalized to the maximum number of contacts observed between two residues. A contact is defined as any heavy atom of the two residues within 5 Å at any time. The important areas of the plot are marked with black ellipses.

Residues Phe15 and Phe23 were some of the first residues to make contact with other peptides in many simulations and they made very persistent interactions with the same aromatic residues of the other peptides. This clear indication of the importance of the hydrophobic and aromatic residues for the initial interaction between the peptides substantiates previous experimental

findings: Mutational studies of full length amylin[67,68] and fragments[69] have shown that aromatic interactions are important for the rate of aggregation, though not a strict requirement for the formation of amyloids. One hypothesis is that these initial aromatic interactions decrease the flexibility of the peptides and make it feasible for the 22-NFGAIL-27 segments of the peptides to approach each other and thereby accelerate the aggregation, which has previously been suggested from NMR experiments and 2D-infrared spectroscopy.[70,71] From the plot of interactions in **Figure 5a** it is seen that interactions with residues 22-NFGAIL-27 are abundant after 100 ns and the diagonal in the contact map (**Figure 5b**) indicate in-register interactions between the peptides in the region of residues 22-NFGAIL-27. In-register interactions in this region are expected to be present in the mature fibrils based on available NMR-ensembles of the fibril and fragments.[72,73] This segment has a strong propensity to aggregate, and has previously been identified as part of the amyloidogenic core of amylin.[69] The observations made here therefore suggest that in the process of fibril formation, the initial contacts involve the aromatic residues after which the 22-NFGAIL-27 segments makes lasting in-register contacts between the peptides.

Conformational changes of the neutral amylin peptides during self-assembly.

Major conformational changes are observed as the peptides interact. In all the starting conformations, the peptide consisted of two α-helices, one near the N-terminus and a smaller one at the C-terminus (**Figure 3b)**, similar to the NMR structure of amylin bound to SDS micelles.[24] The evolution of the average degree of secondary structure during the simulations is shown in **Figure 6a** the secondary structure of each residue is determined with the DSSP algorithm.[74] The degree of α-helix structure generally decayed rapidly within the first 50 ns of the simulations to

less than 10%, while the average degree of β-strand increased to around 5%. The secondary-structure distribution was relatively stable until around 200 ns, where a second noteworthy increase in average degree of β-strand to above 10% occurred. The average distribution of secondary structure for each residue excluding the first 50 ns of the simulations is shown in **Figure 6b**.

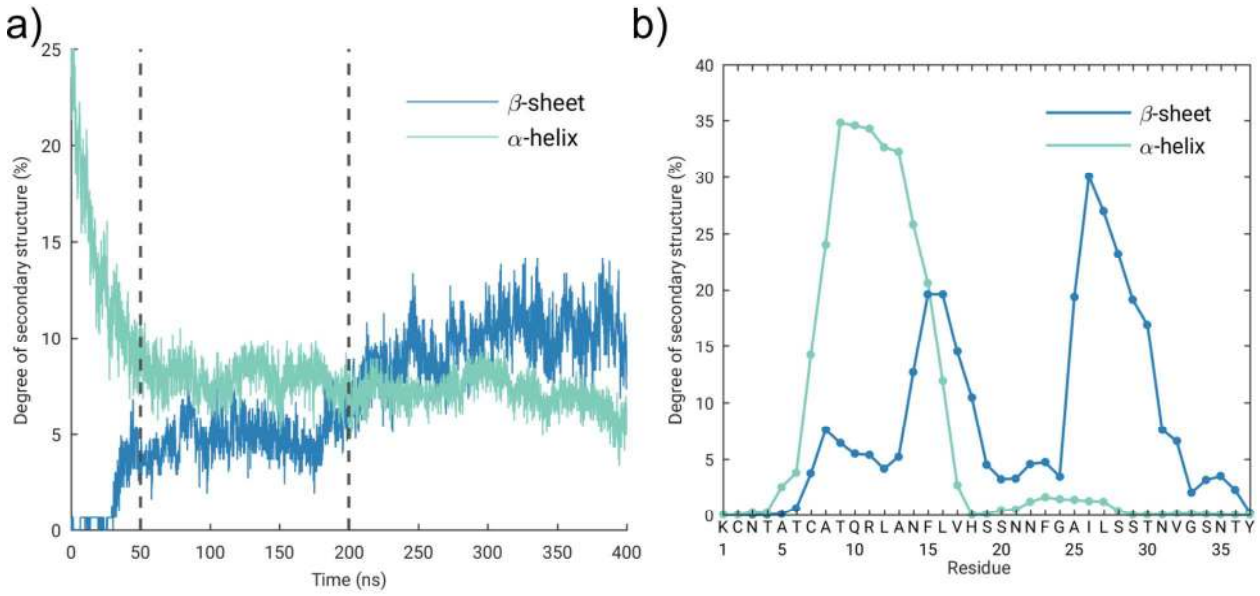

Figure 6: a) Average degree of β-strand and α-helix content of the aggregating peptides during the simulations. The blue curve corresponds to the fraction of residues in β-strand conformation and the green curve corresponds to the fraction of α-helical residues. The dashed lines are located at t=50 ns and t=200 ns. b) Average distribution of β-strand and α-helix content of the aggregating peptides for each residue in the simulations excluding the first 50 ns. The blue curve corresponds to the average fraction of residues in β-strand structure and the green curve corresponds to the average fraction of α-helical residues. The secondary structure is determined with the DSSP algorithm.[74]

The highest degree of α-helix content is present for residues 8 to 16, this helix was present in the starting structure of all peptides in the simulations and it was stabilized by interactions with the membrane. The α-helices unfolded for many of the aggregating peptides, and are only present in 35% of the peptides on average, excluding the first 50 ns, which is seen from **Figure 6**. Since the helices are stable with a single peptide in the previous study,[52] the rapid destabilization is likely due to the change in environment from the presence of other peptides on the bilayer. In some simulations the α-helices unfolded to coiled structures and sometimes it refolded into β-strand conformation. The residues with the highest propensity for forming β-strands in the simulations were residues 14-NFLVH-18 and 25-AILST-30. Residue Ile26 had the highest propensity and was found in β-strand conformation about 30% of the time.

Figure 7 displays the time evolution of the secondary structure of and it is seen that after 200 ns around 40% of the peptides had β-strand in the region of residues 25-AILSST-30 and around 20% in 14-NFLVH-18. The symmetry between the degrees of β-strand formation between these two segments is due to β-hairpin formation. This effect is less pronounced late in the simulations where residues 25-AILSST-30 have the highest degree of β-strand conformation.

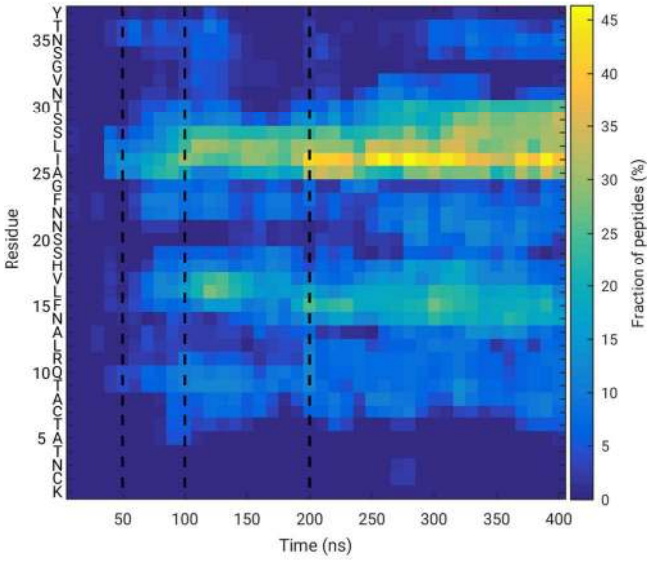

Figure 7: Fraction of peptides with residues in a β-strand conformation as a function of time. The first dashed line indicates t=50 ns and the second t=100 ns, and a third at 200 ns.

A map of the average intra-peptide contacts are shown in **Figure 8**. Intra-peptide contacts are defined here as any C_α atom being within 5 Å of another C_α atom of the same peptide. The N-terminal residues 1-7 are characterized by the disulfide bridge connecting Cys2 and Cys7. The diagonal from the bottom-left represents constant interactions to adjacent, covalently bonded residues, reflecting the peptide chain. This diagonal is broadened from residue Ala8 to His18 which is due to the α-helix present in the starting structure, in which residue i interacts with residue $i \pm 4$ in the next turn. Two anti-diagonals are observed to be dominating in the simulations; the first anti-diagonal (1) in **Figure 8** with contacts between residues Asn14-Ser19 and Phe23-Ser29, and a second (2) with contacts between residues Thr9-Leu16 and His18-Thr30.

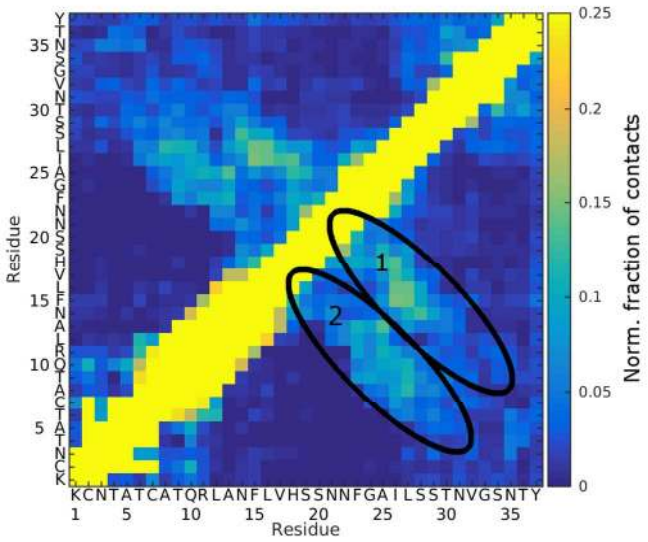

Figure 8: Average intra-peptide contact map of the peptides, showing the normalized fraction of contacts between Cα atoms. Contacts present in more than a 0.25 fraction of the time are shown in yellow. The α-helix is indicated by the broadening of the diagonal from Ala8 to His18. The two anti-diagonals 1 and 2 are indicated.

The anti-diagonals correspond to hairpin structures as was also visually observed in the simulations. The hairpin from anti-diagonal (1) with interactions between residues Asn14-Ser19 and residue Phe23-Ser29 was the most abundant. This hairpin had the same turn as observed in the NMR structures of mature fibrils of amylin, although in the fibril structure the β-sheets are always formed between different peptides, as illustrated in **Figure 2**.[27,72,72,75,75] The presence of the β-hairpin structure in the present study, correlates well with previous experiments and simulations of structural ensembles of monomer amylin, from which it has been hypothesized that the hairpin is a potential pre-nuclear structure.[29,76,77]

Generally, the segment with the highest β-strand propensity in the simulations was 25-AILSST-30 as shown in **Figure 5b**; several of these residues are within the segment with the

most inter-peptide contacts, the 22-NFGAIL-27 segment. This is expected, because this part of the peptide has a high propensity to aggregate into β-sheet containing structures. Mutational studies using ThT binding assays and CD spectroscopy have shown that an Ile26Pro[78] or Gly24Pro[79] mutation can inhibit fibril formation. Furthermore, rat amylin is known not to form amyloid fibrils. It contains only 6 mutations relative to the human variety, of which five are within residues Phe23-Ser29, and three of the substitutions are to prolines: Ala25Pro, Ser28Pro, and Ser29Pro.[80] Proline is a known β-strand breaker and since mutations to proline in this segment would prevent important interactions between the peptides and prevent the initial β-strand formation, it abolishes the amyloid formation, possibly already in this initial stage of the self-assembly.

Peptide-lipid interactions

Throughout the simulations the N-terminal part of the peptides display strong interactions with the membrane and no peptides were observed to dissociate from the membrane surface. **Figure 9** shows the average distance between each residue and the central x-y plane of the membrane.

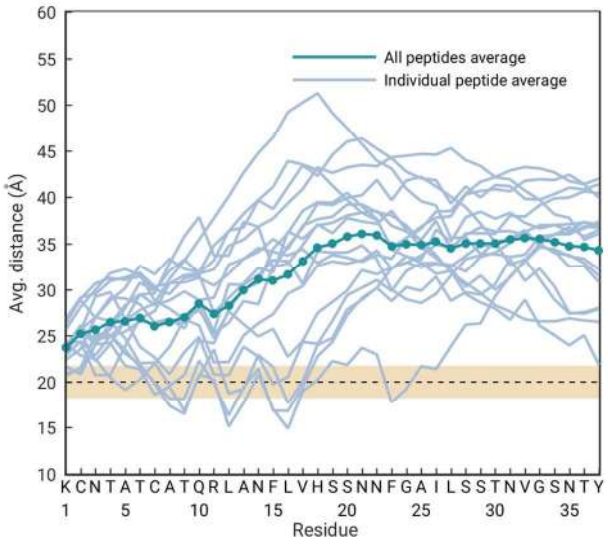

Figure 9: Average distance to membrane center for the 17 peptides having neutral His18 and showing aggregation. The average distance of each residue to the center of the membrane for each peptide is shown in blue, and the average of all the peptides is shown in green. Distance is measured from the central x-y plane of the membrane. The average z-coordinate of the phosphate atoms of the lipids is shown with a dashed line and standard deviation is shown in yellow.

Residues Lys1 to Arg11 were located approximately 25 Å from the center of the membrane, corresponding to within 5 Å of the phosphate groups of the lipids. This is likely caused mainly by the positive charge at the N-terminus, and residues Lys1 and Arg11 interacting with the negatively charged PS lipids. The C-terminal residues His18 to Tyr37 were on average placed nearly 10 Å higher than the N-terminus. From the anchor point at Arg11 towards the C-terminal the residues showed a high degree of flexibility, as seen in the large differences in the z-coordinates for the C-terminal residues of the 17 individual peptides. In the α-helix present in the N-terminus of the starting structures, the hydrophobic residues Ala8, Leu12, Ala13, Phe15, and

Leu16 were pointing into the membrane, whereas the more hydrophilic residues Gln10, Arg11, and Asn14 were pointing toward the solvent. This burying of the hydrophobic residues in the membrane stabilized the N-terminal α-helix and sustained the anchoring of amylin. As shown in **Figure 6** this α-helix was not stable in all the simulations, as it unfolded as the peptides started to interact with one another. In the present study Lys1-Arg11 were mostly bound to the surface of the membrane, and therefore made almost no contact to other peptides, as revealed by **Figure 5**. This is in agreement with experimental data from infrared reflection absorption spectroscopy that a peptide consisting of the 19 N-terminal residues of amylin interact strongly with the membrane and surface tension experiments have also shown that while the N-terminal part interacts strongly with the membrane, the Ser20-Ser29 fragment does not interact with the membrane.[81] Here, the flexible C-terminus had more freedom to sample larger parts of phase space as it is not mounted directly to the membrane. As shown in **Figure 5** the C-terminal part made the most inter-peptide contact, which we suggest is linked to the increased flexibility and the larger distance from the membrane compared to the N-terminal, hereby allowing the peptides to interact.[52] The amount of time the Lys1 residues were in contact with a given PS and PC lipid is shown in **Figure S2.** Almost all the peptides had its Lys1 in contact with the same PS lipids for more than 100 ns and in many cases for more than 300 ns. This is due to a strong electrostatic interaction between the positive charges of the N-terminus and both the carboxylate found in the PS lipid headgroup and with the phosphate of the phospholipid headgroups. In comparison the zwitterionic PC lipids, shown in **Figure S3**, which also have a negative charge at the phosphate part of the head-group, only had interactions with Lys1 for more than 100 ns in a few cases. This indicates that PS lipids have a stronger interaction to the peptides than PC lipids. Having the peptides confined to the two dimensions of the membrane surface instead of a 3-dimensional

solution makes it more likely for the peptides to meet and aggregate. This provides evidence for the hypothesis that the observed speed-up of aggregation in the presence of membrane bilayers with either anionic lipids or gangliosides, which has been suggested to increase the local concentration of amylin.[33]

Simulations with positively charged His18

The peptides with positively charged His18 showed an increased attraction between the peptides and the lipid head groups as compared to peptides with neutral His18. In this set of simulations the N-terminal α-helix is fixed to the lipid-solvent interface by electrostatic interactions with the positively charged residues Lys1 and His18 at the ends of the N-terminal α-helix and in the middle with Arg11. The average distance between the residues of the peptides and the membrane center is shown in **Figure 10**. The residues of the α-helix are buried well below the phosphate layer of the lipids and have much less variation among the peptides than the peptides with neutral His18 (**Figure 9**). The hydrophilic residues of the N-terminal α-helix: Gln10, Arg11, Asn14, and His18 are situated at the level of the phosphates, whereas the hydrophobic residues were pointing into the hydrophobic core of the membrane. This is in contrast to simulations with the neutral His18 where these residues are mostly above the membrane-water interface. The C-terminus of the peptides is more flexible with varying distances to the membrane center for residues 20 to 37, a shorter flexible region than the peptides with neutral His18 (**Figure 9**).

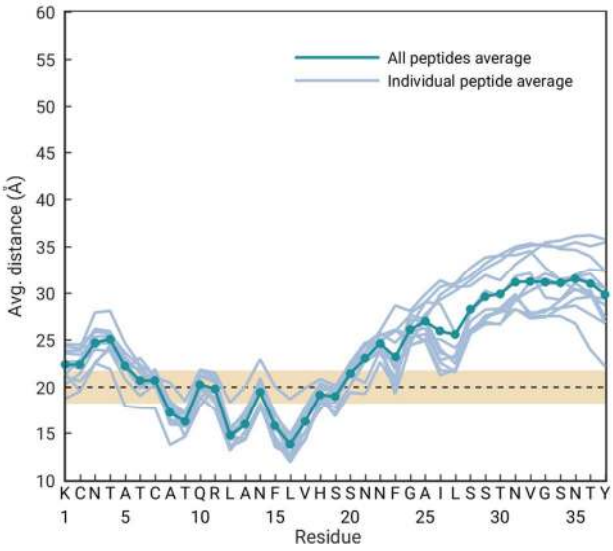

Figure 10: Average distances to the center of the membrane for each residue of the peptides with positively charged His18. The average z-coordinates of the residues in each peptide are plotted in blue, and the average distance of all the peptides is shown in green. Distance is measured from the central x-y plane of the membrane. The average z-coordinate of the phosphate atoms of the lipids is shown with a dashed line and standard deviation is shown in yellow.

Only very little self-assembly was observed for the peptides with positive His18, which is shown in **Figure S1**. The peptides with cationic His18 are more strongly bound to the membrane, than the neutral His18 peptides, which gives less flexible peptides, which is seen in **Figure 10**, and thus preventing the structural changes necessary for self-assembly. Another contributing factor is maybe the increased repulsion between the peptides due to the additional positive charge. The simulations with neutral His18 showed a lot of inter-peptide interaction in the segments close to His18, and the charge-charge repulsion is expected to make this less favorable. For this reason fewer sustained contacts were observed between these peptides. From kinetic experiments with ThT binding assays and CD spectroscopy it has been shown that fibril formation and membrane damage is slowed down in low pH conditions, where His18 is expected

to become protonated.[40,82] The results in the present study hereby suggests that the slow-down occur in the initial self-assembly to inhibit protofibril formation.

CONCLUSIONS

In this study we have shown that the transition from membrane bound α-helical amylin peptides to β-strand containing oligomers is dependent on the protonation state of His18. Aggregation is rapid for the peptides with a neutral His18 and is initiated with interactions between aromatic residues (Phe15 and Phe23) followed by β-sheet formation. The peptides with positively charged His18 did not aggregate. The analysis indicates the following mechanism for the initial phase of amylin self-assembly as sketched in **Figure 11**: a) The peptides diffuse on the membrane with the N-terminus fixed to anionic lipids via electrostatic interaction. The N-terminus is initially α-helical, whereas the C-terminus is found to be flexible. When the peptides start to interact with other peptides, some of the interactions with the membrane are broken and the α-helical structure is partly or fully unfolded, in both the N- and the C-terminal. b) The self-assembly initiates in the central part, and the contacts between the peptides show that the aromatic residues make the initial interactions between the peptides. c) The initial contact with the aromatic residues enables contact in the segment of residues 22-NFGAIL-27, which in several of the simulations make long-lasting interactions similar to interactions found in the known fibril structures. d) When the peptides self-assemble, β-sheets are formed, and the highest propensity for formation of β-strand is observed in residues 14-NFLVH-18 and 25-AILSST-30. Some of the β-strands that are formed are intra-peptide β-hairpin structures while others are part of inter-peptide β-sheets. The β-hairpin conformation has previously been proposed to be a pre-nuclear structure of amylin[75] and the areas with the highest degree of β-strand content fits with experiments as the regions expected to have β-strand in the fibrils.[27]

The simulations with the charged His18 did not reveal any self-assembly, the extra charge makes the anchoring to the membrane additionally strong by increased electrostatic interactions between the positively charged residues and the anionic PS lipids, and thus prevents the conformational changes necessary for self-assembly to take place. The charge at His18 similarly increases the repulsion between the peptides near segments that are important for the interaction between the peptides.

With the results presented here we are able to explain many of the experimental results within amylin structure and aggregation in atomic detail. This time-resolved structural data thus provides detailed knowledge on the interaction between the amylin peptides and membranes during the initial self-assembly. This knowledge can potentially be applied in identifying importing steps in the early aggregation, which can be used as targets in the development of new therapeutics meant to inhibit self-assembly or the interactions with the membrane. Already known inhibitors of amylin aggregation and membrane damage include rifampicin,[83] Congo Red, and other polyphenolic compounds, which possibly work by preventing membrane insertion of the peptide assemblies.[84] Extending the system in size and simulation time could reveal more steps towards fibril formation. Such studies are underway in our group including more complex and physiologically relevant membrane models and more peptides.

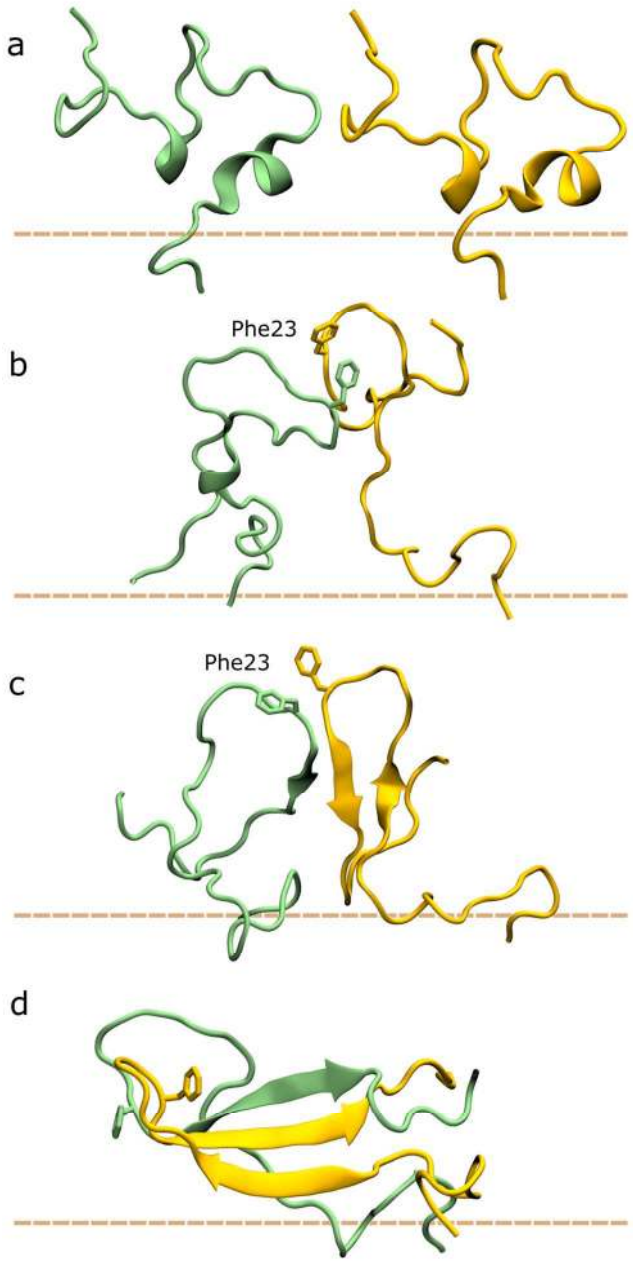

Figure 11: Sketch of the mechanism of amylin self-assembly of two peptides. The peptides are shown in green and orange, respectively. The level of the phospholipid phosphates is sketched as a dashed orange line. (a) Monomer, membrane-bound amylin in α-helix conformation. (b) Peptides unfold and initiate contact to other peptides through aromatic interaction with Phe23. (c) Oligomers are formed with in-register β-sheet formation. (d) The β-strands extend.

Funding information

We thank the Lundbeck foundation, the Sino-Danish Center for education and research, and the Danish Council for independent Research in Technology and Production (FTP) for funding.

ACKNOWLEDGEMENT

Computations were made possible by the Centre for Scientific Computing Aarhus (CSCAA). Dr. Mikkel Vestergaard is acknowledged for valuable discussions.

SUPPORTING INFORMATION AVAILABLE

Figure S1: Number of residues in contact between peptides

Figure S2: Interactions between Lys1 and PS lipids

Figure S3: Interaction between Lys1 and PC lipids

Movie S1: Simulation trajectory with 4 peptides self-assembling

Movie S2: Simulation trajectory with 3 peptides self-assembling

Movie S3: Simulation trajectory with no peptide self-assembly

REFERENCES

1. Lukinius, A., Wilander, E., Westermark, G. T., Engstrom, U., and Westermark, P. (1989) Co-localization of islet amyloid polypeptide and insulin in the B cell secretory granules of the human pancreatic-islets. *Diabetologia 32*, 240-244.

2. Lutz, T. A. (2012) Control of energy homeostasis by amylin. *Cell. Mol. Life Sci. 69*, 1947-1965.

3. Maloy, A. L., Longnecker, D. S., and Robert Greenberg, E. (1981) The relation of islet amyloid to the clinical type of diabetes. *Hum. Pathol. 12*, 917-922.

4. Zhao, H. L., Lai, F. M. M., Tong, P. C. Y., Zhong, D. R., Yang, D., Tomlinson, B., and Chan, J. C. N. (2003) Prevalence and clinicopathological characteristics of islet amyloid in chinese patients with type 2 diabetes. *Diabetes 52*, 2759-2766.

5. Höppener, J. W., Ahrén, B., and Lips, C. J. (2000) Islet amyloid and type 2 diabetes mellitus. *N. Engl. J. Med. 343*, 411-419.

6. Jurgens, C. A., Toukatly, M. N., Fligner, C. L., Udayasankar, J., Subramanian, S. L., Zraika, S., Aston-Mourney, K., Carr, D. B., Westermark, P., and Westermark, G. T. (2011) B-cell loss and β-cell apoptosis in human type 2 diabetes are related to islet amyloid deposition. *Am. J. Pathol. 178*, 2632-2640.

7. Stumvoll, M., Goldstein, B. J., and van Haeften, T. W. (2007) Pathogenesis of type 2 diabetes. *Endocr. Res. 32*, 19-37.

8. Westermark, P., Andersson, A., and Westermark, G. T. (2011) Islet amyloid polypeptide, islet amyloid, and diabetes mellitus. *Physiol. Rev. 91*, 795-826.

9. Sparr, E., Engel, M., Sakharov, D., Sprong, M., Jacobs, J., de Kruijff, B., Hoppener, J., and Killian, J. (2004) Islet amyloid polypeptide-induced membrane leakage involves uptake of lipids by forming amyloid fibers. *FEBS Lett. 577*, 117-120.

10. Engel, M. F. M., Khemtémourian, L., Kleijer, C. C., Meeldijk, H. J. D., Jacobs, J., Verkleij, A. J., de Kruijff, B., Killian, J. A., and Höppener, J. W. M. (2008) Membrane damage by human islet amyloid polypeptide through fibril growth at the membrane. *Proc. Natl. Acad. Sci. U. S. A. 105*, 6033-6038.

11. Engel, M. F. M. (2009) Membrane permeabilization by islet amyloid polypeptide. *Chem. Phys. Lipids 160*, 1-10.

12. Quist, A., Doudevski, L., Lin, H., Azimova, R., Ng, D., Frangione, B., Kagan, B., Ghiso, J., and Lal, R. (2005) Amyloid ion channels: A common structural link for protein-misfolding disease. *Proc. Natl. Acad. Sci. U. S. A. 102*, 10427-10432.

13. Mirzabekov, T., Lin, M., and Kagan, B. (1996) Pore formation by the cytotoxic islet amyloid peptide amylin. *J. Biol. Chem. 271*, 1988-1992.

14. Last, N. B., Rhoades, E., and Miranker, A. D. (2011) Islet amyloid polypeptide demonstrates a persistent capacity to disrupt membrane integrity. *Proc. Natl. Acad. Sci. U.S.A. 108*, 9460-9465.

15. Anguiano, M., Nowak, R. J., and Lansbury, P. T. (2002) Protofibrillar islet amyloid polypeptide permeabilizes synthetic vesicles by a pore-like mechanism that may be relevant to type II diabetes. *Biochemistry 41*, 11338-11343.

16. Scalisi, S., Sciacca, M. F. M., Zhavnerko, G., Grasso, D. M., Marletta, G., and La Rosa, C. (2010) Self-assembling pathway of HiApp fibrils within lipid bilayers. *ChemBioChem 11*, 1856-1859.

17. Khemtémourian, L., Doménech, E., Doux, J. P. F., Koorengevel, M. C., and Killian, J. A. (2011) Low pH acts as inhibitor of membrane damage induced by human islet amyloid polypeptide. *J. Am. Chem. Soc. 133*, 15598-15604.

18. Williamson, J. A., Loria, J. P., and Miranker, A. D. (2009) Helix stabilization precedes aqueous and bilayer-catalyzed fiber formation in islet amyloid polypeptide. *J. Mol. Biol. 393*, 383-396.

19. Williamson, J. A., and Miranker, A. D. (2007) Direct detection of transient α-helical states in islet amyloid polypeptide. *Protein Sci. 16*, 110-117.

20. Caillon, L., Lequin, O., and Khemtémourian, L. (2013) Evaluation of membrane models and their composition for islet amyloid polypeptide-membrane aggregation. *Biochim. Biophys. Acta, Biomembr. 1828*, 2091-2098.

21. Knight, J. D., Hebda, J. A., and Miranker, A. D. (2006) Conserved and cooperative assembly of membrane-bound α-helical states of islet amyloid polypeptide. *Biochemistry 45*, 9496-9508.

22. Knight, J. D., Williamson, J. A., and Miranker, A. D. (2008) Interaction of membrane-bound islet amyloid polypeptide with soluble and crystalline insulin. *Protein Sci. 17*, 1850-1856.

23. Patil, S. M., Xu, S., Sheftic, S. R., and Alexandrescu, A. T. (2009) Dynamic α-helix structure of micelle-bound human amylin. *J. Biol. Chem. 284*, 11982-11991.

24. Nanga, R. P. R., Brender, J. R., Vivekanandan, S., and Ramamoorthy, A. (2011) Structure and membrane orientation of IAPP in its natively amidated form at physiological pH in a membrane environment. *Biochim. Biophys. Acta, Biomembr. 1808*, 2337-2342.

25. Goldsbury, C. S., Cooper, G. J. S., Goldie, K. N., Müller, S. A., Saafi, E. L., Gruijters, W. T. M., Misur, M. P., Engel, A., Aebi, U., and Kistler, J. (1997) Polymorphic fibrillar assembly of human amylin. *J. Struct. Biol. 119*, 17-27.

26. Goldsbury, C., Goldie, K., Pellaud, J., Seelig, J., Frey, P., Muller, S. A., Kistler, J., Cooper, G. J. S., and Aebi, U. (2000) Amyloid fibril formation from full-length and fragments of amylin. *J. Struct. Biol. 130*, 352-362.

27. Luca, S., Yau, W., Leapman, R., and Tycko, R. (2007) Peptide conformation and supramolecular organization in amylin fibrils: Constraints from solid-state NMR. *Biochemistry 46*, 13505-13522.

28. Dupuis, N. F., Wu, C., Shea, J. E., and Bowers, M. T. (2009) Human islet amyloid polypeptide monomers form ordered beta-hairpins: A possible direct amyloidogenic precursor. *J. Am. Chem. Soc. 131*, 18283-18292.

29. Dupuis, N. F., Wu, C., Shea, J. E., and Bowers, M. T. (2011) The amyloid formation mechanism in human IAPP: Dimers have β-strand monomer-monomer interfaces. *J. Am. Chem. Soc. 133*, 7240-7243.

30. Lee, C., Sun, Y., and Huang, H. W. (2012) How type II diabetes-related islet amyloid polypeptide damages lipid bilayers. *Biophys. J. 102*, 1059-1068.

31. Jayasinghe, S., and Langen, R. (2005) Lipid membranes modulate the structure of islet amyloid polypeptide. *Biochemistry 44*, 12113-12119.

32. Knight, J. D., and Miranker, A. D. (2004) Phospholipid catalysis of diabetic amyloid assembly. *J. Mol. Biol. 341*, 1175-1187.

33. Wakabayashi, M., and Matsuzaki, K. (2009) Ganglioside-induced amyloid formation by human islet amyloid polypeptide in lipid rafts. *FEBS Lett. 583*, 2854-2858.

34. Amaro, M., Šachl, R., Aydogan, G., Mikhalyov, I. I., Vácha, R., and Hof, M. (2016) GM1 ganglioside inhibits β-amyloid oligomerization induced by sphingomyelin. *Angew. Chem. Int. Ed. 55*, 9411-9415.

35. Cho, W., Trikha, S., and Jeremic, A. M. (2009) Cholesterol regulates assembly of human islet amyloid polypeptide on model membranes. *J. Mol. Biol. 393*, 765-775.

36. Trikha, S., and Jeremic, A. M. (2011) Clustering and internalization of toxic amylin oligomers in pancreatic cells require plasma membrane cholesterol. *J. Biol. Chem. 286*, 36086-36097.

37. Caillon, L., Duma, L., Lequin, O., and Khemtemourian, L. (2014) Cholesterol modulates the interaction of the islet amyloid polypeptide with membranes. *Mol. Membr. Biol. 31*, 239-249.

38. Lopes, D. H. J., Meister, A., Gohlke, A., Hauser, A., Blume, A., and Winter, R. (2007) Mechanism of islet amyloid polypeptide fibrillation at lipid interfaces studied by infrared reflection absorption spectroscopy. *Biophys. J. 93*, 3132-3141.

39. Hutton, J. C. (1982) The internal pH and membrane-potential of the insulin-secretory granule. *Biochem. J. 204*, 171-178.

40. Abedini, A., and Raleigh, D. P. (2005) The role of his-18 in amyloid formation by human islet amyloid polypeptide. *Biochemistry 44*, 16284-16291.

41. Nilsson, M. R. (2004) Techniques to study amyloid fibril formation in vitro. *Methods 34*, 151-160.

42. Mo, Y., Lei, J., Sun, Y., Zhang, Q., and Wei, G. (2016) Conformational ensemble of hIAPP dimer: Insight into the molecular mechanism by which a green tea extract inhibits hIAPP aggregation. *Sci. Rep. 6*, 33076.

43. Chebaro Y, Jiang P, Zang T, Mu Y, Nguyen PH, Mousseau N, Derreumaux P. (2012) Structures of Aβ17–42 trimers in isolation and with five small-molecule drugs using a hierarchical computational procedure. *J. Phys. Chem. B 116 (29)*, 8412-8422.

44. Poojari, C., Xiao, D., Batista, V. S., and Strodel, B. (2013) Membrane permeation induced by aggregates of human islet amyloid polypeptides. *Biophys. J. 105*, 2323-2332.

45. Sørensen, J., Periole, X., Skeby, K. K., Marrink, S. J., and Schiøtt, B. (2011) Protofibrillar assembly toward the formation of amyloid fibrils. *J. Phys. Chem. B 2*, 2385-2390.

46. Karplus, M., and McCammon, J. A. (2002) Molecular dynamics simulations of biomolecules. *Nat. Struct. Mol. Biol. 9*, 646-652.

47. Ohkubo, Y. Z., Pogorelov, T. V., Arcario, M. J., Christensen, G. A., and Tajkhorshid, E. (2012) Accelerating membrane insertion of peripheral proteins with a novel membrane mimetic model. *Biophys. J. 102*, 2130-2139.

48. Vermaas, J. V., and Tajkhorshid, E. (2014) A microscopic view of phospholipid insertion into biological membranes. *J. Phys. Chem. B 118*, 1754-1764.

49. Vermaas, J. V., and Tajkhorshid, E. (2014) Conformational heterogeneity of α-synuclein in membrane. *Biochim. Biophys. Acta, Biomembr. 1838*, 3107-3117.

50. Baylon, J. L., and Tajkhorshid, E. (2015) Capturing spontaneous membrane insertion of the influenza virus hemagglutinin fusion peptide. *J. Phys. Chem. B 119*, 7882-7893.

51. Baylon, J. L., Lenov, I. L., Sligar, S. G., and Tajkhorshid, E. (2013) Characterizing the membrane-bound state of cytochrome P450 3A4: Structure, depth of insertion, and orientation. *J. Am. Chem. Soc. 135*, 8542-8551.

52. Skeby, K. K., Andersen, O. J., Pogorelov, T. V., Tajkhorshid, E., and Schiøtt, B. (2016) Conformational dynamics of the human islet amyloid polypeptide in a membrane environment: Toward the aggregation prone form. *Biochemistry 55*, 2031-2042.

53. Zhang, X., St Clair, J. R., London, E., and Raleigh, D. P. (2017) Islet amyloid polypeptide membrane interactions: Effects of membrane composition. *Biochemistry 56*, 376-390.

54. Neria, E., Fischer, S., and Karplus, M. (1996) Simulation of activation free energies in molecular systems. *J. Chem. Phys. 105*, 1902-1921.

55. MacKerell Jr., A. D., Bashford, D., Bellott, M., Dunbrack Jr., R. L., Evanseck, J. D., Field, M. J., Fischer, S., Gao, J., Guo, H., Ha, S., Joseph-McCarthy, D., Kuchnir, L., Kuczera, K., Lau, F. T. K., Mattos, C., Michnick, S., Ngo, T., Nguyen, D. T., Prodhom, B., Reiher III, W. E., Roux, B., Schlenkrich, M., Smith, J. C., Stote, R., Straub, J., Watanabe, M., Wiórkiewicz-Kuczera, J., Yin, D., and Karplus, M. (1998) All-atom empirical potential for molecular modeling and dynamics studies of proteins. *J. Phys. Chem. B 102*, 3586-3616.

56. Jorgensen, W. L., Chandrasekhar, J., Madura, J. D., Impey, R. W., and Klein, M. L. (1983) Comparison of simple potential functions for simulating liquid water. *J. Chem. Phys. 79*, 926-935.

57. Abraham, M. J., Murtola, T., Schulz, R., Páll, S., Smith, J. C., Hess, B., and Lindahl, E. (2015) GROMACS: High performance molecular simulations through multi-level parallelism from laptops to supercomputers. *SoftwareX 1–2*, 19-25.

58. Klauda, J. B., Venable, R. M., Freites, J. A., O'Connor, J. W., Tobias, D. J., Mondragon-Ramirez, C., Vorobyov, I., MacKerell, A. D., and Pastor, R. W. (2010) Update of the CHARMM all-atom additive force field for lipids: Validation on six lipid types. *J. Phys. Chem. B 114*, 7830-7843.

59. Piana, S., Lindorff-Larsen, K., and Shaw, D. (2011) How robust are protein folding simulations with respect to force field parameterization? *Biophys. J. 100*, L47-L49.

60. Hoffmann, K. Q., McGovern, M., Chiu, C. C., and de Pablo, J. J. (2015) Secondary structure of rat and human amylin across force fields. *PLoS One 10*, e0134091.

61. Carballo-Pacheco, M., and Strodel, B. (2017) Comparison of force fields for alzheimer's A β42: A case study for intrinsically disordered proteins. *Protein Science 26*, 174-185.

62. Hess, B., Bekker, H., Berendsen, H. J. C., and Fraaije, J. G. E. M. (1997) LINCS: A linear constraint solver for molecular simulations. *J. Comput. Chem. 18*, 1463-1472.

63. Bussi, G., Donadio, D., and Parrinello, M. (2007) Canonical sampling through velocity rescaling. *J. Chem. Phys. 126*, 014101.

64. Parrinello, M., and Rahman, A. (1981) Polymorphic transitions in single crystals: A new molecular dynamics method. *J. Appl. Phys. 52*, 7182-7190.

65. Essmann, U., Perera, L., Berkowitz, M. L., Darden, T., Lee, H., and Pedersen, L. G. (1995) A smooth particle mesh ewald method. *J. Chem. Phys. 103*, 8577-8593.

66. Steinbach, P. J., and Brooks, B. R. (1994) New spherical-cutoff methods for long-range forces in macromolecular simulation. *J. Comput. Chem. 15*, 667-683.

67. Marek, P., Abedini, A., Song, B., Kanungo, M., Johnson, M. E., Gupta, R., Zaman, W., Wong, S. S., and Raleigh, D. P. (2007) Aromatic interactions are not required for amyloid fibril formation by islet amyloid polypeptide but do influence the rate of fibril formation and fibril morphology. *Biochemistry 46*, 3255-3261.

68. Tu, L., and Raleigh, D. P. (2013) Role of aromatic interactions in amyloid formation by islet amyloid polypeptide. *Biochemistry 52*, 333-342.

69. Azriel, R., and Gazit, E. (2001) Analysis of the minimal amyloid-forming fragment of the islet amyloid polypeptide: An experimental support for the key role of the phenylalanine residue in amyloid formation. *J. Biol. Chem. 276*, 34156-34161.

70. Shim, S., Gupta, R., Ling, Y. L., Strasfeld, D. B., Raleigh, D. P., and Zanni, M. T. (2009) Two-dimensional IR spectroscopy and isotope labeling defines the pathway of amyloid formation with residue-specific resolution. *Proc. Natl. Acad. Sci. 106*, 6614-6619.

71. Wei, L., Jiang, P., Xu, W., Li, H., Zhang, H., Yan, L., Chan-Park, M. B., Liu, X. W., Tang, K., Mu, Y., and Pervushin, K. (2011) The molecular basis of distinct aggregation pathways of islet amyloid polypeptide. *J. Biol. Chem. 286*, 6291-6300.

72. Kajava, A. V., Aebi, U., and Steven, A. C. (2005) The parallel superpleated beta-structure as a model for amyloid fibrils of human amylin. *J. Mol. Biol. 348*, 247-252.

73. Nielsen, J. T., Bjerring, M., Jeppesen, M. D., Pedersen, R. O., Pedersen, J. M., Hein, K. L., Vosegaard, T., Skrydstrup, T., Otzen, D., and Nielsen, N. C. (2009) Unique identification of supramolecular structures in amyloid fibrils by solid-state NMR spectroscopy. *Angew. Chem., Int. Ed. 48*, 2118-2121.

74. Kabsch, W., and Sander, C. (1983) Dictionary of protein secondary structure: Pattern recognition of hydrogen-bonded and geometrical features. *Biopolymers 22*, 2577-2637.

75. Nagel-Steger, L., Owen, M. C., and Strodel, B. (2016) An account of amyloid oligomers: Facts and figures obtained from experiments and simulations. *ChemBioChem 17*, 657-676.

76. Singh, S., Chiu, C., Reddy, A. S., and de Pablo, J. J. (2013) A-helix to β-hairpin transition of human amylin monomer. *J. Chem. Phys. 138*, 155101.

77. Reddy, A. S., Wang, L., Singh, S., Ling, Y. L., Buchanan, L., Zanni, M. T., Skinner, J. L., and de Pablo, J. J. (2010) Stable and metastable states of human amylin in solution. *Biophys. J. 99*, 2208-2216.

78. Abedini, A., Meng, F., and Raleigh, D. P. (2007) A single-point mutation converts the highly amyloidogenic human islet amyloid polypeptide into a potent fibrillization inhibitor. *J. Am. Chem. Soc. 129*, 11300-11301.

79. Meng, F., Raleigh, D. P., and Abedini, A. (2010) Combination of kinetically selected inhibitors in trans leads to highly effective inhibition of amyloid formation. *J. Am. Chem. Soc. 132*, 14340-14342.

80. Cao, P., Marek, P., Noor, H., Patsalo, V., Tu, L., Wang, H., Abedini, A., and Raleigh, D. P. (2013) Islet amyloid: From fundamental biophysics to mechanisms of cytotoxicity. *FEBS Lett. 587*, 1106-1118.

81. Engel, M. F. M., Yigittop, H., Elgersma, R. C., Rijkers, D. T. S., Liskamp, R. M. J., de Kruijff, B., Höppener, J. W. M., and Killian, J. A. (2006) Islet amyloid polypeptide inserts into phospholipid monolayers as monomer. *J. Mol. Biol. 356*, 783-789.

82. Jha, S., Snell, J. M., Sheftic, S. R., Patil, S. M., Daniels, S. B., Kolling, F. W., and Alexandrescu, A. T. (2014) pH dependence of amylin fibrillization. *Biochemistry 53*, 300-310.

83. Harroun, T. A., Bradshaw, J. P., and Ashley, R. H. (2001) Inhibitors can arrest the membrane activity of human islet amyloid polypeptide independently of amyloid formation. *FEBS Lett. 507*, 200-204.

84. Pillay, K., and Govender, P. (2013) Amylin uncovered: A review on the polypeptide responsible for type II diabetes. *Biomed. Res. Int. 2013*, 826706.

For Table of Contents Use Only

Identification of Key Interactions in the Initial Self-Assembly of Amylin in a Membrane Environment

Mikkel Christensen, Katrine K. Skeby, and Birgit Schiøtt